# Internal Tides over a Shelf Break: Analytical Model and Observations

A. PICHON

*Service Hydrographique et Océanographique de la Marine, Brest.*

R. MAZÉ

*Université de Bretagne Occidentale, Brest.*

(Manuscript received 9 February 1989, in final form 3 November 1989)

ABSTRACT

Data collected on Cruise ONDINE 85 organized by the Service Hydrographique et Océanographique de la Marine, at two points ($P_1$ and $P_6$) near the continental shelf break of the Bay of Biscay, show very large amplitudes of internal tides. These waves exhibit a strong nonlinear character of the semidiurnal evolution of the thermocline depth. During spring tide, the internal oscillations can reach 80 meters.

In order to get an analytical solution for the interface depth variation near the top of the shelf break, the two layer nonlinear model of generation and propagation of internal tides developed by Mazé is linearized in the present paper.

Taking account of several monochromatic tides waves ($M_2$, $S_2$, $N_2$, $K_2$) in the forcing term, comparison between this analytical solution and data can be done over a six-week period. Such a comparison shows that the scale of the interface level and the time variation of the interface are quite well reproduced by the analytical model.

## 1. Introduction

It is well known that tidal movement over a significant topographical feature creates internal waves of large amplitude. The dynamics of these waves, their action on the various physical sea processes, and consequently the theories used to describe them differ depending on whether the movements are generated over a continental sill or slope.

Where there is a sill, the tidal current can, in general, be assumed to be alternating and weak on either side of the barrier. It is formed, on the ebb, a solitary wave which, during its movement, develops into a group of solitons, creating a change in the roughness of the sea. This surface change has been observed in the Andaman Sea by satellite (Osborne and Burch 1980) and more recently in the Sulu Sea (Apel 1985b). These theories describe the transformation of a solitary wave into a wave group, neglecting the rotation of the earth and the influence of the time variations of the barotropic current on its movement.

Where internal waves are generated over a continental slope, if the current is weak over the abyssal plain, it is strong over the shelf; consequently the time variation of the barotropic current and rotation effects can no longer be neglected.

The slope of the Bay of Biscay is a prime zone for the formation of this type of internal wave (Baines 1982). Numerous observations (Pingree et al. 1983; Mazé et al. 1986) have shown both that the wave amplitude is large over the continental edge of the slope, and that the deformation of these waves during their movement over the shelf seems to be due to interaction between internal waves and barotropic waves. To describe the formation and movement mechanisms of these internal tides, a two-layer model has been constructed; this model is based on the fact that the movement of the tide over the slope causes the existence of a vertical component of the associated current (Mazé 1987). If the ocean is layered, a forced oscillation of the interface, which creates a pressure gradient in the bottom layer, then appears at the edge of the slope. The internal waves thus formed move along both sides of the slope. This model has been only briefly tested against data.

The object of this study is to interpret recent observations (carried out during the S.H.O.M. ONDINE 85 cruise) of internal tides on the edge of the Bay of Biscay continental slope. This interpretation is based on an analytical model that describes the internal oscillation in the formation zone.

After a brief review of the assumptions and theoretical concepts underpinning this model (Mazé 1987), the analytical expression is tested against two sets of data obtained over a period of one and a half months from thermistor chains placed at two points near the continental shelf break.

*Corresponding author address:* Dr. Annick Pichon, Section Oceanographie, EPSHOM, 13, Rue du Chatellier, B.P. 426, 29275 Brest Cedex, France.

## 2. Theory

The model used is in two layers and unidirectional following a radial $O_x$, perpendicular to the slope.

The symbols for the variables are as follows (Fig. 1):

| | |
|---|---|
| $\vec{U}(U, V)$ | barotropic current |
| $\vec{U}_1(u_1, v_1)$ | horizontal baroclinic current in the surface layer (1) |
| $\vec{U}_2(u_2, v_2)$ | horizontal baroclinic current in the bottom layer (2) |
| $h_0$ | average depth of the thermocline |
| $\xi$ | barotropic vertical displacement of the free surface |
| $\eta_1$ | baroclinic vertical displacement of the free surface |
| $\eta$ | baroclinic vertical displacement of the interface |
| $h$ | $h = h_0 - \eta$ |
| $\rho_1, \rho_2$ | density of the surface (1) and bottom (2) layers |
| $g'$ | $g' = g[(\rho_2 - \rho_1)/\rho_2]$ reduced gravity |
| $H$ | total depth |
| $a$ | $a = -(dH/dx)$ slope |

### a. *Basic equations*

Assumptions:

1) The spatial variations of the variables along $O_y$ (parallel to the slope) are neglected.

2) In the analytical model, only one non-linear term is introduced: the transport of the internal wave by the barotropic current, $U$, across the slope.

3) The gradient of the barotropic free surface vertical displacements $\overrightarrow{\text{grad}}\,\xi$, is assumed to be negligible with respect to the gradients of the baroclinic vertical displacements ($\overrightarrow{\text{grad}}\,\eta$ and $\overrightarrow{\text{grad}}\,\eta_1$).

4) The baroclinic free surface vertical displacement, $\eta_1$, is assumed to be related to the baroclinic thermocline vertical displacement, $\eta$, by:

$$\overrightarrow{\text{grad}}\,\eta_1 = \frac{g'}{g}\frac{H-h}{H}\overrightarrow{\text{grad}}\,h \quad (h = h_0 - \eta) \text{ (Mazé 1987)}$$

(This assumption is the generalization of the well-known relation for a first-mode internal wave over a flat bottom.)

With these simplifying assumptions, the motion and continuity equations (integrated into the bottom layer), become:

$$\frac{\partial u_1}{\partial t} + U\frac{\partial u_1}{\partial x} - fv_1 = -g'\frac{H-h}{H}\frac{\partial h}{\partial x} \quad (1)$$

$$\frac{\partial v_1}{\partial t} + U\frac{\partial v_1}{\partial x} + fu_1 = 0 \quad (2)$$

$$\frac{\partial u_2}{\partial t} + U\frac{\partial u_2}{\partial x} - fv_2 = g'\frac{h}{H}\frac{\partial h}{\partial x} \quad (3)$$

$$\frac{\partial v_2}{\partial t} + U\frac{\partial v_2}{\partial x} + fu_2 = 0 \quad (4)$$

$$\frac{\partial h}{\partial t} + U\frac{\partial h}{\partial x} = -a\frac{Uh}{H} + \frac{\partial((H-h)u_2)}{\partial x}. \quad (5)$$

Equation (5) shows the internal wave formation mechanism: the forcing term, $a(Uh/H)$, is the vertical component of the barotropic current at the depth $h$. The important spatial variations of this term near the shelf break, involve a spatial variation of the thermocline depth and therefore generate horizontal pressure gradients which generate the internal motion.

The internal wave generation is assumed to be produced at the point where the forcing term is maximum, i.e. on the continental shelf break. This hypothesis introduces an uncertainty on the phase internal motion owing to the fact that there is not only one generation point but rather a zone of generation along the continental slope.

### b. *Change in the baroclinic interface level, $\eta(t)$, at points on the continental edge of the slope, for a monochromatic barotropic current of frequency $\omega$*

According to linear theory, an internal wave moves over the continental shelf with a phase velocity given by

$$C_0^2 = g'\frac{h(H-h)}{H}\Big/\left(1 - \frac{f^2}{\omega^2}\right).$$

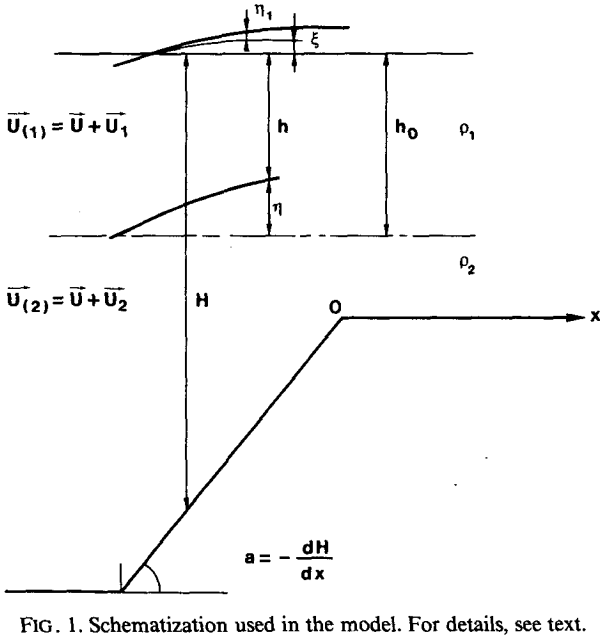


FIG. 1. Schematization used in the model. For details, see text.

When wave transport by barotropic current is introduced, the velocity over the shelf becomes

$$C = U + C_0.$$

The baroclinic variables $\eta$, $u_1$, $v_1$, $u_2$, $v_2$, $\eta_1$ of the form $Ke^{j\omega\left[t-\left(x-\int_0^t U(\tau)d\tau\right)/C_0\right]}$ satisfy the equation system (1) to (4).

The amplitudes of the baroclinic currents $u_1$ and $u_2$ (perpendicular to the slope) are then related to the interface vertical displacement by the equations:

$$u_1 = -C_0\eta/h, \quad u_2 = C_0\eta/(H-h).$$

These equations remain valid for points on the slope near the break ($x = 0$).

If the spatial variation of $C_0$ and the influence of $\eta$ in the forcing term, a $(Uh/H)$, and in $C_0$, are assumed to be negligible, Eq. (5) becomes

$$\frac{\partial\eta}{\partial t} + (U + C_0)\frac{\partial\eta}{\partial x} = a\frac{Uh_0}{H}$$

with

$$C_0^2 = g'\frac{h_0(H-h_0)}{H}\Big/\left(1-\frac{f^2}{\omega^2}\right).$$

According to the results of the numerical model (Mazé 1987), on the shelf break, the baroclinic interface level change is proportional to the barotropic current:

$$\eta \approx \frac{U}{\omega}e^{F(x,t)} \rightarrow \frac{\partial\eta}{\partial x} \approx \left(\frac{a}{H}+\frac{\partial F}{\partial x}\right)\eta \qquad (6)$$

$$(1) \quad (2)$$

where $a/H$ represent the spatial variations of the forced wave and $\partial F/\partial x$ the spatial variation associated with the progressive wave character.

On the slope near the shelf break, the spatial variation of the progressive wave (2) is negligible in relation to that of the forced wave (1) (Mazé 1987).

The time variation of $\eta$ is given by the following equation:

$$\frac{\partial\eta}{\partial t} + (U + C_0)\frac{a}{H}\eta = a\frac{Uh_0}{H}.$$

On the continental shelf break, for $x = 0$, the time variation of $\eta$ has the form:

$$\eta(t) = \frac{ah_0}{H}e^{-(a/H)\left(C_0t+\int_0^t U(\tau')d\tau'\right)} \times \int_0^t U(\tau)e^{(a/H)\left(C_0\tau+\int_0^\tau U(\tau')d\tau'\right)}d\tau. \quad (7)$$

This solution will henceforth be referred to as $\eta_T(t)$.

*c. Introduction of several waves of differing frequencies into the forcing term*

With a harmonic analysis, the component of the barotropic current perpendicular to the slope can be written as

$$U(t) = \sum_{i=1}^{n} U_i f(\omega_i, t).$$

Each contribution of the barotropic current creates an interface depth variation, $\eta_i(\omega_i, t)$, which satisfies the equation:

$$\frac{\partial\eta_i}{\partial t} + (U(t) + C_i)\frac{\partial\eta_i}{\partial x} = \frac{a}{H}h_0U(i)f(\omega_i, t)$$

with

$$C_i^2 = g'\frac{h_0(H-h_0)}{H}\Big/\left(1-\frac{f^2}{\omega_i^2}\right).$$

(In the advection term, $U(t)(\partial\eta_i/\partial x)$, the barotropic current is taken into account totally.)

Given that, $\eta = \sum_{i=1}^{n}\eta_i$ is the total interface depth variation corresponding to the sum of the variations, and that $\eta_i$, resulting from a forcing term, $(a/H)h_0U_if(\omega_i, t)$ of frequency $\omega_i$. Then $\eta$ satisfies the equation:

$$\frac{\partial\eta}{\partial t} + \frac{aU(t)}{H}\eta + \frac{a}{H}\sum_{i=1}^{n} C_i\eta_i = \frac{ah_0}{H}U(t).$$

In the Bay of Biscay the tide is semidiurnal. In the harmonic decomposition of the current, only waves $M_2$, $S_2$, $N_2$, and $K_2$ will be taken into account. These belong to the semidiurnal group and have similar frequencies, $\omega_1$ to $\omega_4$ respectively.

The relative difference between these various frequencies is at most

$$\frac{\Delta\omega}{\omega} \approx 0.06.$$

Let $C_1$ be the phase velocity of wave $M_2$ and $\Delta C_i = C_i - C_1$, the deviation of the phase velocity between the $M_2$ wave and the other waves. The above equation becomes

$$\frac{\partial\eta}{\partial t} + \frac{aU(t)}{H}\eta + \frac{a}{H}(C_1\eta + \sum_{i=1}^{4}\Delta C_i\eta_i) = \frac{ah_0}{H}U(t).$$

Assuming

$$A = \sum_{i=1}^{4}\Delta C_i\eta_i, \quad B = C_i\eta.$$

Given that the level differences $\eta_i$, are approximately proportional to the components, $U_i$:

$$\frac{A}{B} \leqslant 0.3\frac{\max(\Delta C)}{C_1},$$

but

$$\frac{\partial C_i}{C_i} = -\frac{\partial \omega_i}{\omega_i}(\omega_i^2/f_i^2 - 1)^{-1},$$

hence

$$\frac{|\Delta C_i|}{C_i} \approx \frac{|\Delta \omega_i|}{\omega_i} \approx 0.06$$

$$\frac{A}{B} \leqslant 0.02.$$

$\sum_{i=1}^{4} \Delta C_i \eta_i$ is negligible when compared to $C_1\eta$.

It can therefore be admitted that all four waves considered move with velocity $C_1$.

The total interface level difference, $\eta$, at a point on the slope near $x = 0$ changes over time according to solution (7) (section 2b) with

$$U(t) = \sum_{i=1}^{4} U_i f(\omega_i, t).$$

*d. Change in the interface baroclinic level, $\eta(t)$, near the shelf break*

On the continental shelf at a short distance, $x$, from the shelf break, the forcing term, $a(Uh_0/H)$, is null. ($a = 0$ on the continental shelf, see Fig. 1)

Equation (5) (section 2a) becomes

$$\frac{\partial \eta}{\partial t} + (U + C_1)\frac{\partial \eta}{\partial x} = 0$$

where $\partial\eta/\partial x$ now represents only the spatial variation of the progressive wave [Eq. (6), section 2b].

The solution of this equation has the form:

$$\eta_P(x, t) = f\left(t - \frac{1}{C_1}\left(x - \int_0^t U(\tau)d\tau\right)\right) = f\left(t - \frac{X}{C_1}\right)$$

where

$$X = x - \int_0^t U(\tau)d\tau$$

is the position of a point in a mobile reference system moving at the velocity of the barotropic current.

$$\eta_P(x, t) = f\left(t - \frac{X}{C_1}\right) = f(t')$$

with

$$t' = t - \frac{x}{C_1} + \int_0^t \frac{U(\tau)}{C_1}\,d\tau$$

hence

$$\eta_P(x, t) = \eta_P(0, t').$$

Because of the continuity condition, the solution for $x = 0$ on the shelf is equal to the solution for $x = 0$ on the slope: $f(t') = \eta_T(0, t')$ [solution (7), section 2b]. Hence

$$\eta_p(x, t) = \eta_P(0, t') = \eta_T(0, t').$$

The diagram (Fig. 2) represents the change in $\eta$ versus time, in a moving (1) and fixed (2) reference system.

When $U$ is in the direction of the propagation, the internal wave is accelerated, but when $U$ is in the opposite direction, the internal wave is braked. This explains the internal wave distortion in the fixed reference system.

In conclusion, the change over time of $\eta_P$ at a point on the shelf at a distance $x$ from the shelf break is given by

$$\eta_P(x, t) = \frac{ah_0}{H} e^{-(a/H)\left(C_1 t' + \int_0^{t'} U(\tau)d\tau\right)} \times \int_0^{t'} U(\tau) e^{(a/H)\left(C_1\tau + \int_0^{\tau} U(\tau')d\tau'\right)} d\tau \quad (8)$$

with

$$t' = t - \frac{x}{C_1} + \int_0^t \frac{U(\tau)}{C_1}\,d\tau$$

$$U(t) = \sum_{i=1}^{4} U_i f(\omega_i, t)$$

where $C_1$ is the phase velocity of the group of four semidiurnal waves.

This expression (8) will now be tested against data in the following section.

## 3. Comparison with data

During the ONDINE 85 cruise (September to November 1985), two moorings, $P_1$ and $P_6$, with thermistor chains and Aanderaa current meters were deployed near the continental shelf break (Fig. 3).

The analytical expression (8) (section d) was tested over one and a half months with measurements taken at $P_1$ and $P_6$. The parameters of the analytical expression are $a$: edge slope, $x$: distance between measuring point and the shelf break, $h_0$: average depth of the interface, $U(t)$: barotropic current across the slope, and $C_1$: phase velocity (depending on hydrological factors).

*a. Introduction of the parameters*

1) CURRENT PERPENDICULAR TO THE SLOPE

In expression (8), $U(t)$ is the component of the barotropic current perpendicular to the slope. At point $P_1$, three current meters have been deployed (during September and October) at different heights: 24 m, 110 m and 158 m (or 12 m off the bottom).

The current across the slope measured at these three heights is plotted (Fig. 4), for a spring tide cycle (from 12 to 18 September).

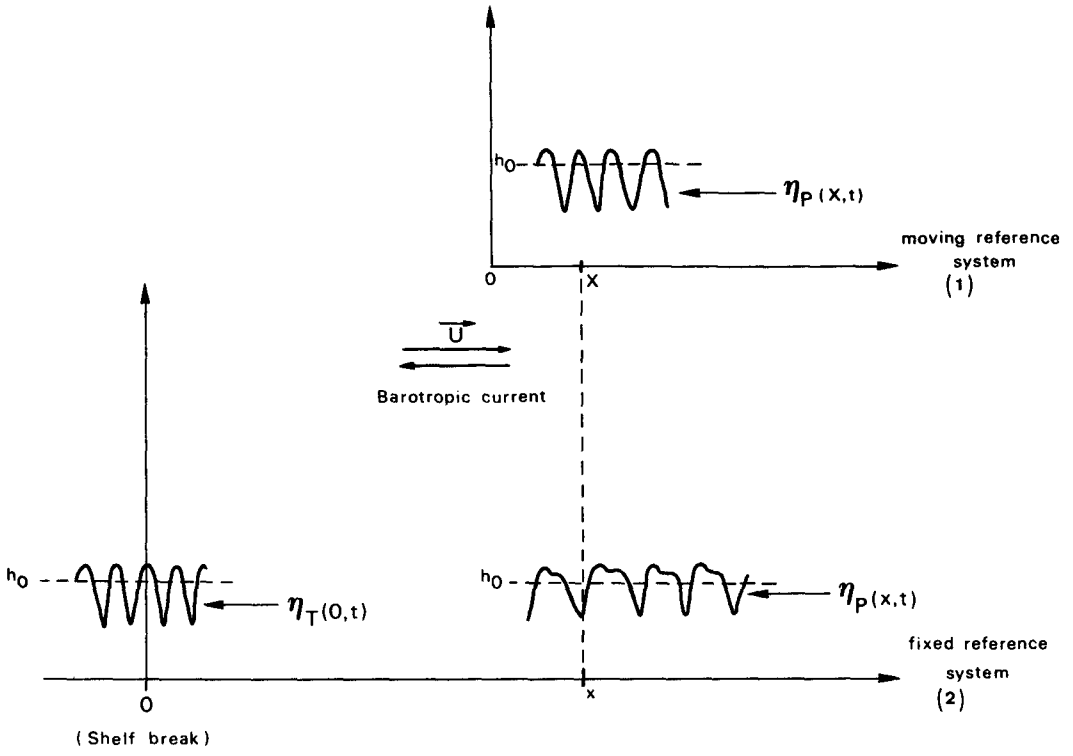


FIG. 2. Barotropic current effect upon the internal wave shape.

At 24 and 158 m the measurements show perturbations into the semidiurnal cycle of the current (see the arrows) induced by the internal wave (Heathershaw et al. 1987).

At 110 m these perturbations are much weaker.

Thus, it seems that the height 110 m is near the depth where the baroclinic current, due to the internal wave, changes direction (in theory; the baroclinic currents at the sea surface and at the bottom are out of phase).

Therefore, the current measured at 110 m will henceforth be considered as representing the barotropic current measurement.

A harmonic analysis of the current measurements at 110 m at $P_1$ and $P_6$ allows the extraction of the representative constants of the semidiurnal waves, $M_2$, $S_2$, $N_2$, $K_2$ (Fig. 5):

| | | $a$ (cm s$^{-1}$) | $b$ (cm s$^{-1}$) | $\beta$ (deg) | $g$ (deg) |
|---|---|---|---|---|---|
| Point $P_1$ | $M_2$ | 47.9 | −21.9 | 29.6 | 61.0 |
| | $S_2$ | 16.3 | −7.4 | 30.4 | 96.8 |
| | $N_2$ | 9.1 | −4.1 | 30.3 | 39.7 |
| | $K_2$ | 4.5 | −2.0 | 31.1 | 92.3 |
| Point $P_6$ | $M_2$ | 49.1 | −28.2 | 36.5 | 73.1 |
| | $S_2$ | 18 | −9.7 | 35.8 | 108.8 |
| | $N_2$ | 10 | −5.4 | 35.9 | 51.8 |
| | $K_2$ | 5.1 | −2.7 | 35.7 | 108.4 |

Let $\theta$ be the angle between the isobath normal and north. The component of the current across the slope, for a wave of frequency $\omega_i$, is

$$U_i(t) = A_i \cos(\omega_i t + \varphi_i) + B_i \sin(\omega_i t + \varphi_i)$$

with

$$A_i = a_i \sin\left(\theta + \frac{\pi}{2} - \beta\right), \quad B_i = b_i \cos\left(\theta + \frac{\pi}{2} - \beta\right)$$

$$\varphi_i = V_i - g_i.$$

Here $V_i$ is the astronomic argument of a wave frequency $\omega_i$ at time $t = 0$. According to the bathymetric data at $P_1$ and $P_6$: $\theta_{P1} = 30°$; $\theta_{P6} = 55°$.

The current introduced into the analytical model will then be the sum of the contribution of the four waves given above:

$$U(t) = \sum_{i=1}^{4} U_i(t).$$

### 2) INTRODUCTION OF THE HYDROLOGICAL PARAMETERS $h_0$, $g'$ AND $C_1$

Over one and one half months, the parameters $h_0$ and $g'$ can vary with the meteorological conditions, so that their actual time variations must be taken into consideration. Their values were determined with the thermistor chain data.

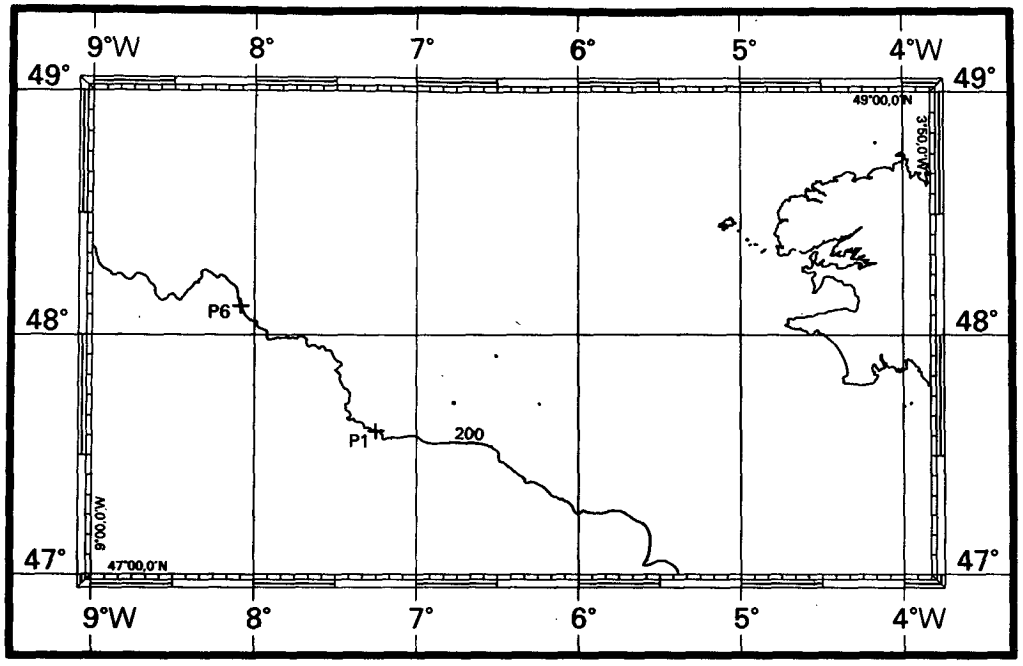


(a)

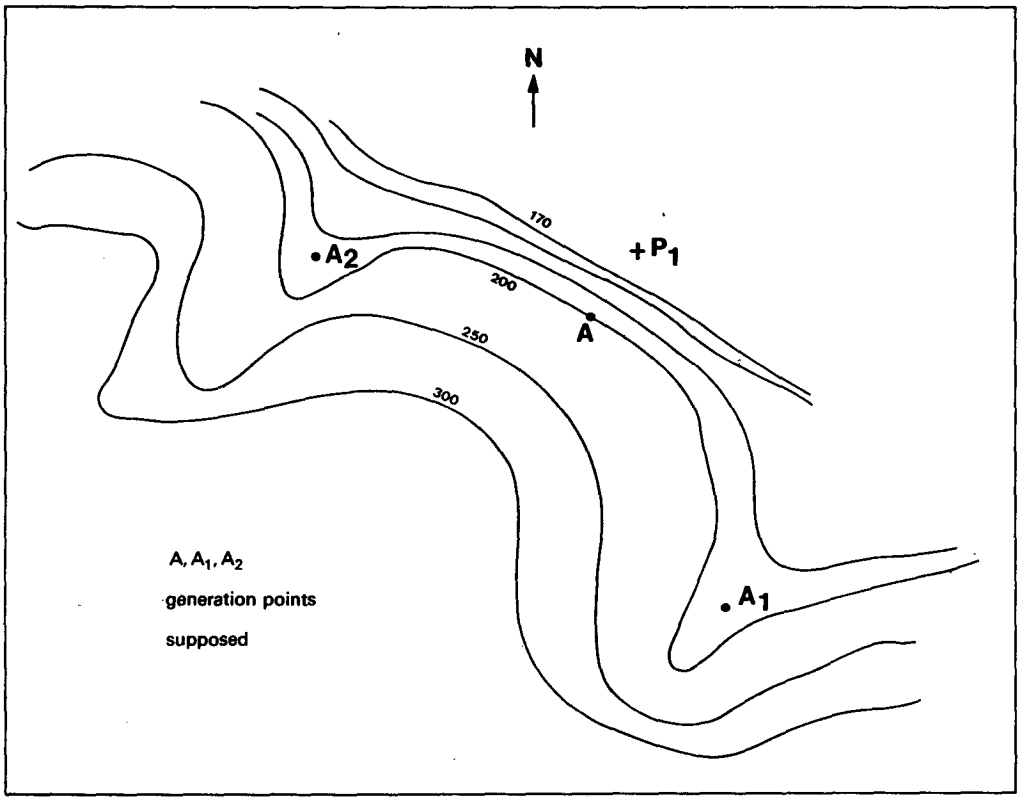


(b)

FIG. 3. (a) Geographical positions of mooring $P_1$ and $P_6$. (b) Bathymetric contours in the vicinity of mooring $P_1$.

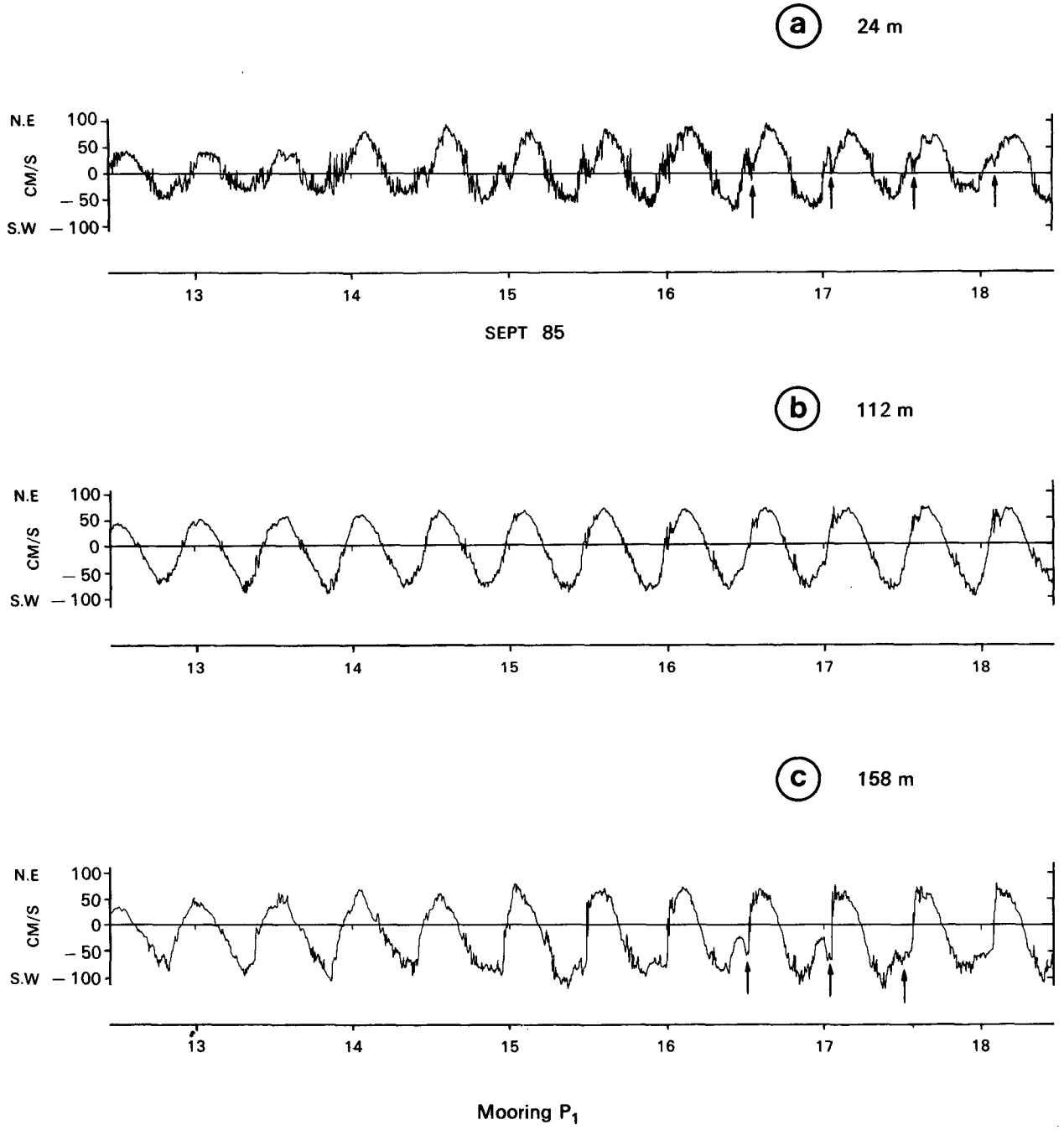


FIG. 4. Mooring $P_1$. Current across the slope measured at 24 m (a), 112 m (b), 158 m (c) during a spring tide period.

Different treatments of the temperature data (low-pass filters eliminating tide frequencies) give the average change in $g'$, $h_1$ and $h_2$ (high and low thermocline depth from the sea surface).

The evolution versus time of $h_1$ and $h_2$ is given by the average depth (over the tidal cycle) of isotherms representative of the thermocline (Figs. 6b and 7b).

The variation of $C_1$, $U(t)$, $g'$, $h_1$, $h_2$, versus time at points $P_1$ and $P_6$ is shown in Figs. 6 and 7. These variations shows that during September and October the thermal structure was usually in three layers. Consequently, in order to conform to the assumptions of a two-layer model, the mean level of the interface $h_0$ is calculated by making the phase velocity of a three-layer model

$$C^2 = g' \frac{h_1(H - (h_1 + h_2)/2)}{H}(1 - f^2/\omega^2)$$

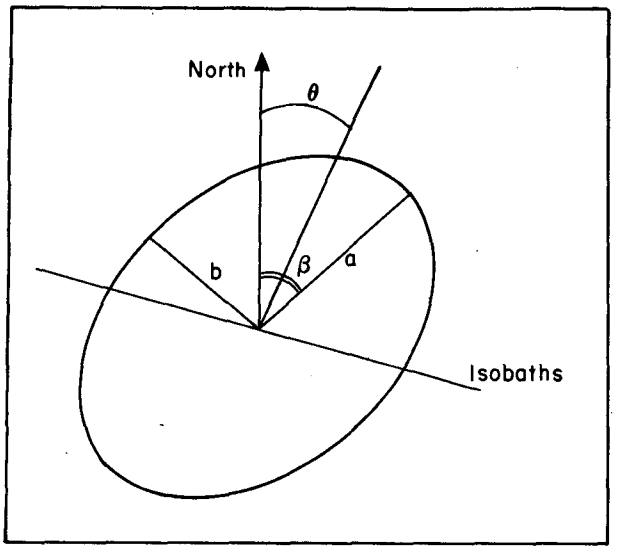


FIG. 5. Representative constants for a tide wave.

equivalent to the phase velocity $C_1$ of a two-layer model:
Thus

$$h_0 = \frac{H}{2} - \frac{[(H - 2h_1)^2 + 2h_1(h_2 - h_1)]^{1/2}}{2}.$$

3) INTRODUCTION OF PARAMETERS $a$ AND $x$

It will be assumed here that the internal wave measured at $P_1$ and $P_6$ is generated at a point on isobath 200 as close as possible to the places of measurement (point A for $P_1$, Fig. 3).

The slope $a$ is an average value calculated between isobaths 200 and 600.

In this case, the parameters have the following values at $P_1$ and $P_6$:

$$P_1: \quad x = 1 \text{ km}, \quad a = 0.06;$$

$$P_6: \quad x = 1.4 \text{ km}, \quad a = 0.025.$$

*b. Results*

The measurements obtained with thermistor chains at $P_1$ and $P_6$, provide the variation over time of isotherms representative of the thermocline during September and October 1985. A part of these temperature data is plotted with the measures of the current across the slope at 110 m (Fig. 8).

The gap between different isotherms shows a change in the thermocline slope during the spring–neap cycle (Fig. 8). For spring tides the thermal structure is best represented by a two-layer model. For neap tides a three-layer model is preferable.

The amplitude of the current measured is the same at $P_1$ and $P_6$ and the phase difference is of the order of 20 minutes. From this it seems highly probable that the current measured at 110 m is a fair representation of the barotropic current.

On the other hand, if we consider now, the phase difference between the internal wave and the barotropic current, it will be noted that at $P_6$, the onset of the internal wave crest and the flood tide maximum are in phase (or within 12.5 h), while at $P_1$ the internal wave is 11 h behind (or 1.5 h ahead of) the current. This is incompatible with the fact that the two points are placed at approximately the same distance from the assumed generation point. (The phase difference between the internal wave and the barotropic current contains a term $\varphi = X/C_1$, which depends on the position of the point in the mobile reference system moving with the barotropic current.)

1) ANALYTICAL RESULTS AT $P_1$

At first, the analytical solution has been tested at point $P_1$ during the third leg, 29 September–6 October 1985, to determine the influence of the various terms of the solution on the wave deformation:

$$C_1 \approx 0.8 \text{ m s}^{-1}, \; h_0 \approx 40 \text{ m},$$

$$8 \times 10^{-3} \text{ m s}^{-2} \leqslant g' \leqslant 1.2 \times 10^{-2} \text{ m s}^{-2}, \quad a \approx 0.06.$$

The first result (Fig. 9a) corresponds to the model solution for a point on the slope at $x = 0$, $\eta_T(0, t)$ [Eq. (7), section 2b]. The introduction of the forced wave spatial variation only [term (1) of Eq. (6)] induces a dissymetric sinusoidal variation of the interface compared with the average depth $h_0$ (a result already observed, Mazé 1987).

Figures 9b and 9c show the interface variation $\eta_P(x, t)$ at a point on the shelf at a distance $x = 1$ km from the shelf break. In a fixed reference system the gap between $\eta_P(x, t)$ and $\eta_P(0, t)$ is

$$\frac{x}{C_1} - \int_0^t \frac{U(\tau)}{C_1} d\tau \quad \text{(cf. section 2d)}.$$

The gap between $\eta_P(x, t)$ and $\eta_P(0, t)$, a function of

$$\int_0^t \frac{U(\tau)}{C_1} d\tau,$$

thus depends on the barotropic current phase $U(\tau)$ chosen at time $t = 0$, and hence on the phase difference between the barotropic current and the internal wave.

This induces a deformation of the internal wave $\eta_P(x, t)$ which is completely different depending on whether the barotropic current is at the onset of flood-tide (Fig. 9b) or the onset of ebb tide at $t = 0$ (Fig. 9c).

The experimental results of Pingree et al. (1986) have been used as a basis to remove the indetermination of the phase difference between the barotropic current and the internal wave.

These results show that the trough of the internal

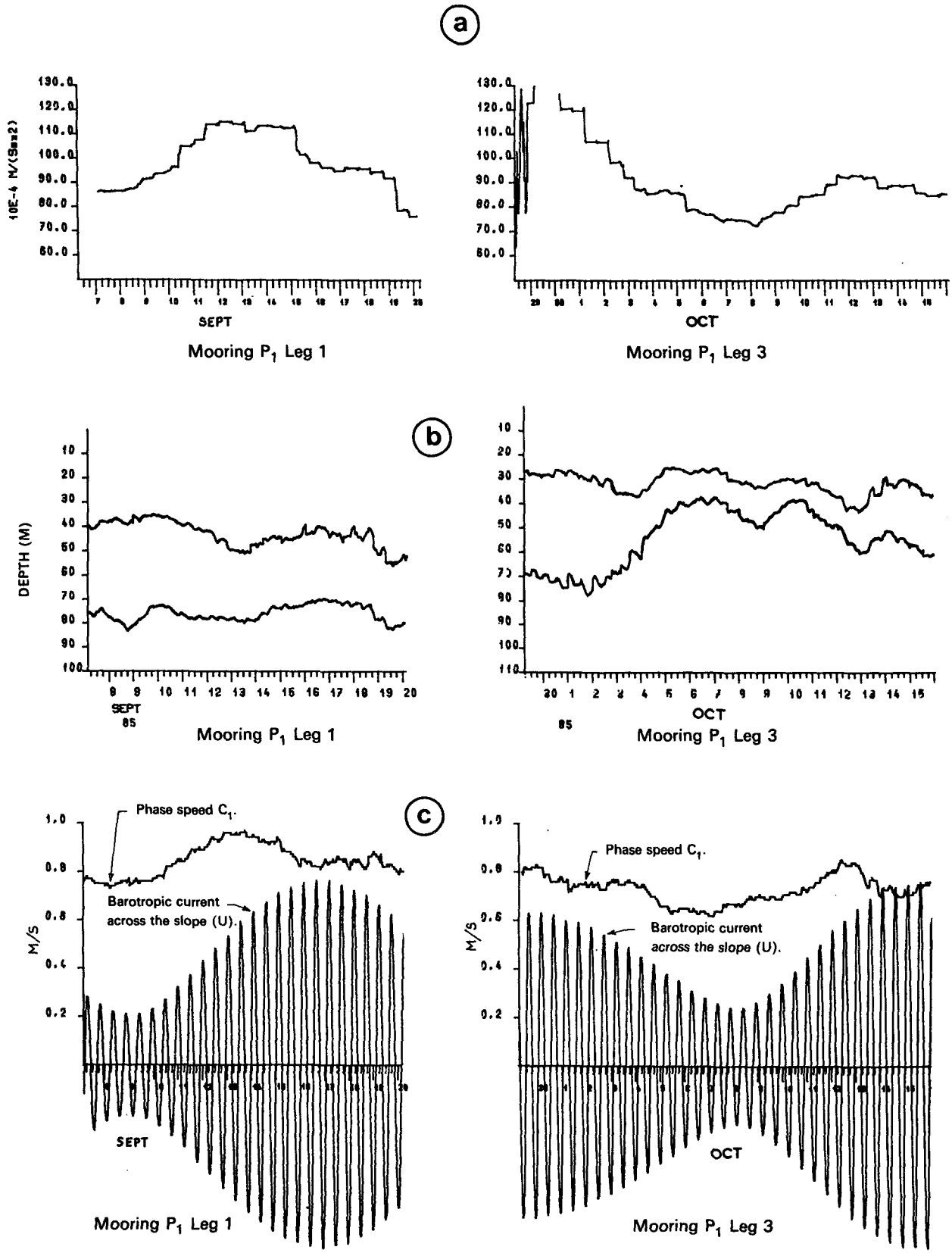


FIG. 6. (a) Variation of reduced gravity, $g'$, versus time at $P_1$. (b) Variation of the mean level of the top ($h_1$) and the bottom ($h_2$) thermocline, versus time at $P_1$. (c) Variation of barotropic current across the slope, $U$, and phase speed $C_1$, versus time at $P_1$.

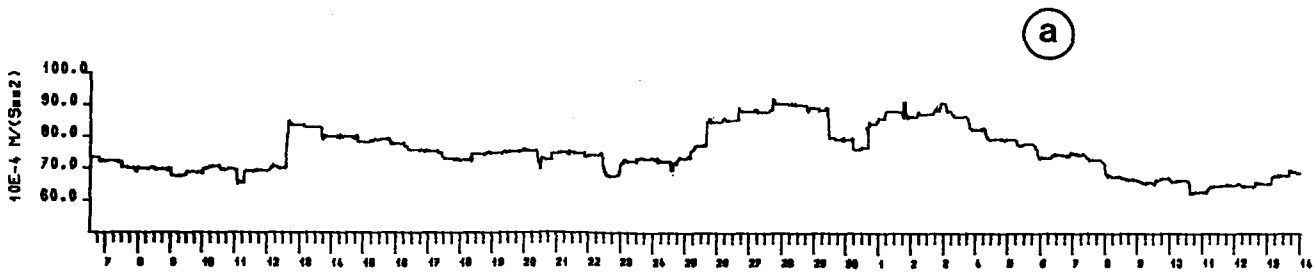


Mooring $P_6$.

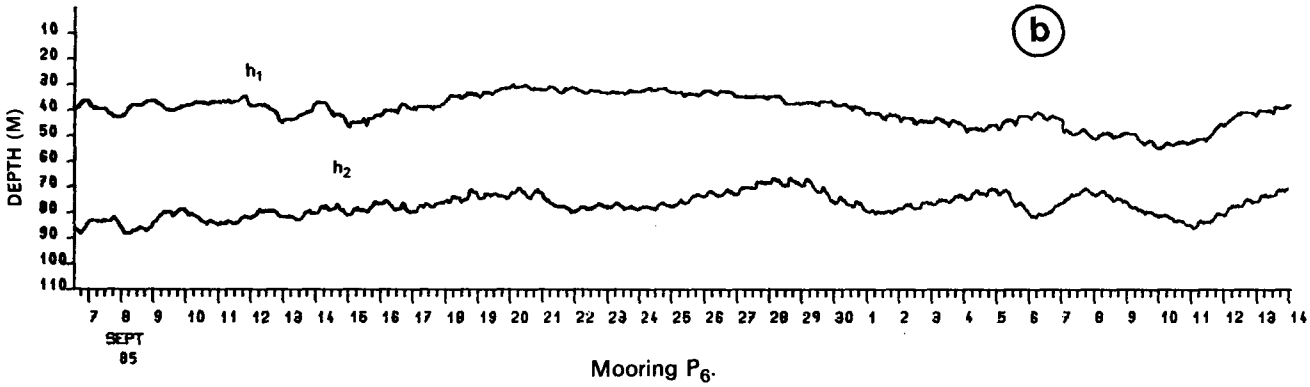


Mooring $P_6$.

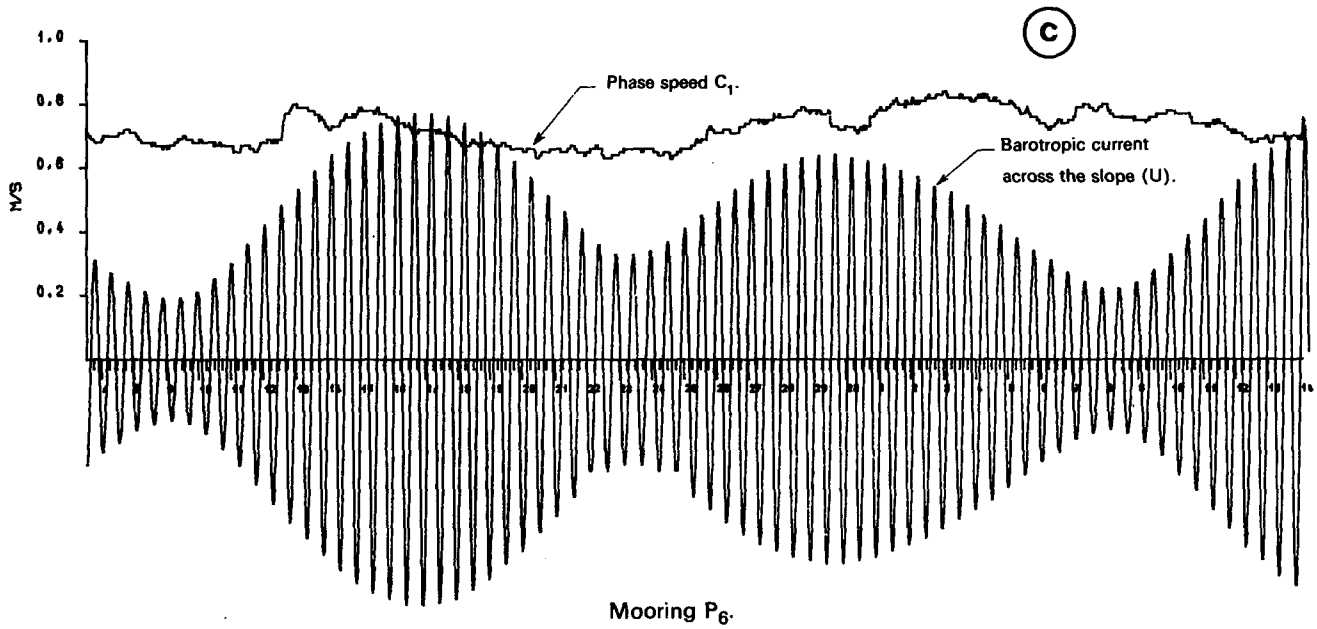


Mooring $P_6$.

FIG. 7. As in Fig. 6, but for $P_6$.

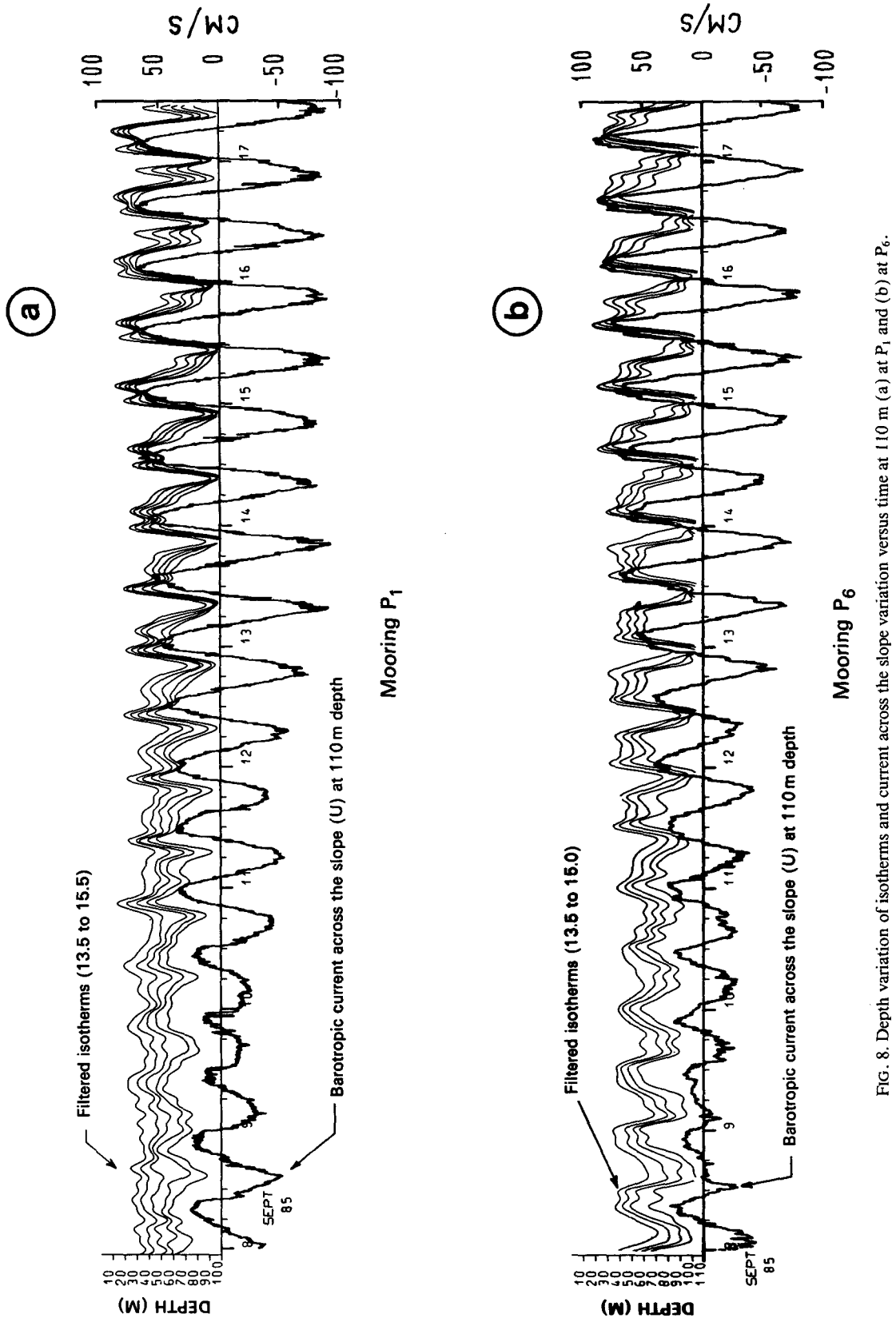


FIG. 8. Depth variation of isotherms and current across the slope variation versus time at 110 m (a) at $P_1$ and (b) at $P_6$.

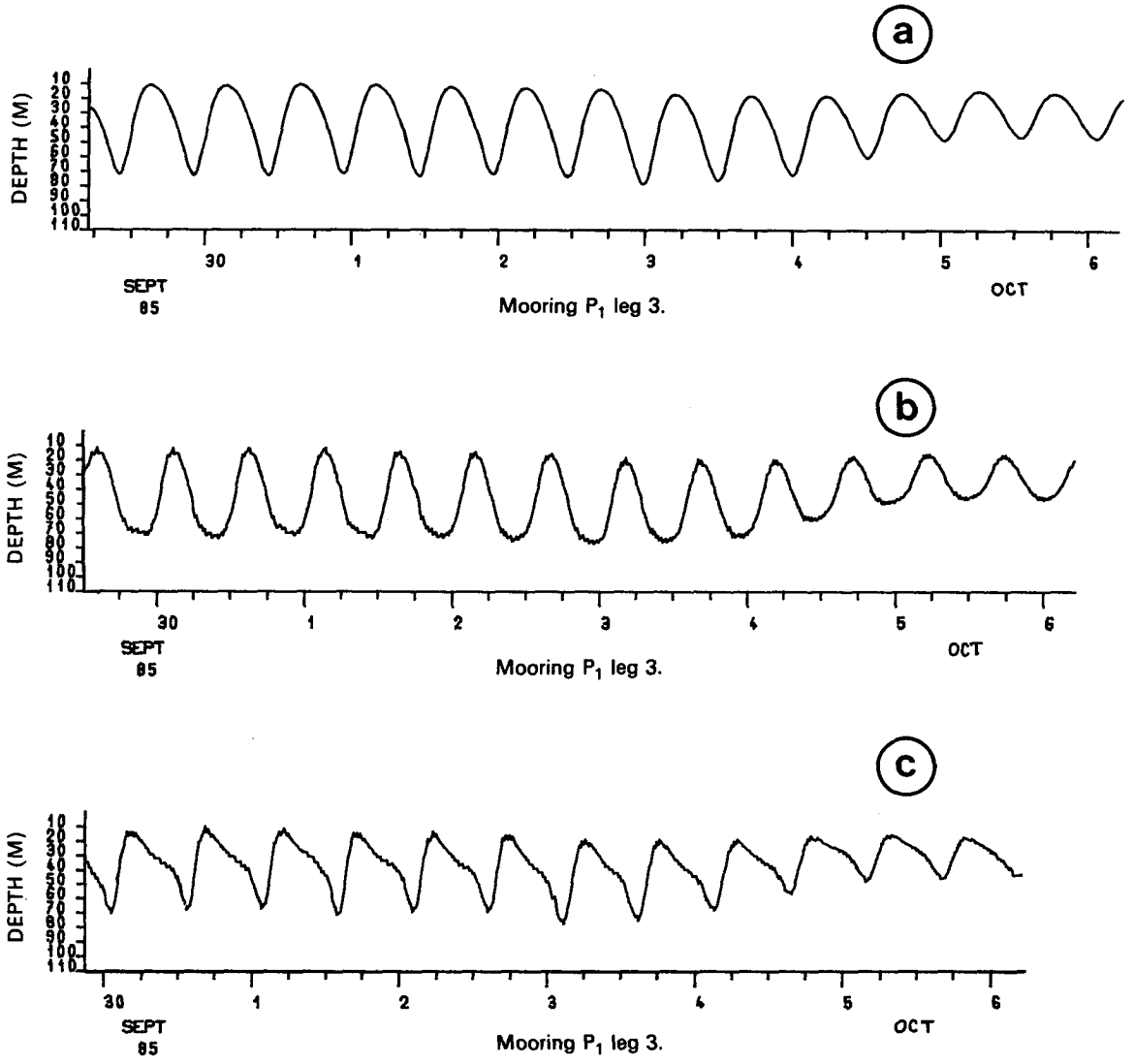


FIG. 9. (a) Interface depth variation versus time as described by modeling at $x = 0$. (b) Interface depth variation versus time as described by modeling at $x = 1$ km, with $U$ at the beginning of the flow at $t = 0$. (c) Interface depth variation versus time as described by modeling at $x = 1$ km, with $U$ at the beginning of the ebb at $t = 0$.

wave is in phase with the full ebb tide or at most two hours behind, which is perfectly consistent with the model result for $t = 0$, where the barotropic current is at the onset of the ebb tide (Fig. 9). This result will therefore serve below in testing the model against data.

The analytical solution is represented together with data for leg 1 (8–17 September) and leg 3 (30 September–13 October) at point $P_1$ (Fig. 10). The comparison of the model with data proves positive for the order of size of the interface depth variation and the shape of the wave at spring tides or high tidal coefficients (14.09–17.09 and 30.09–2.10). On the other hand, at neap tides or low coefficients, the depth variation obtained is lower than the real value. It is possible that this could be improved by adopting a three-layer model of thermal structure.

Since the shape of the internal wave is linked to

$$t_1 = \frac{x}{C_1} - \int_0^t \frac{U(\tau)}{C_1}\, d\tau,$$

the differences in shape observed during legs 1 and 3 for the same tidal coefficient are due to variations in $g'$, $h_1$ and $h_2$ leading to modifications in the phase $C_1$ velocity (in September $C_1 > 0.8$ m s$^{-1}$, in October $C_1 \leq 0.8$ m s$^{-1}$; see Fig. 6).

Moreover, it will be noted that the internal wave calculated with the analytical model is 10.5 h ahead (or 2 h behind) the data. This phase difference is of the same order as that observed between the bottom current and temperature data (Fig. 8). This could be explained by an error in the assumed position of the generation point near $P_1$. Indeed, since it is on the edge

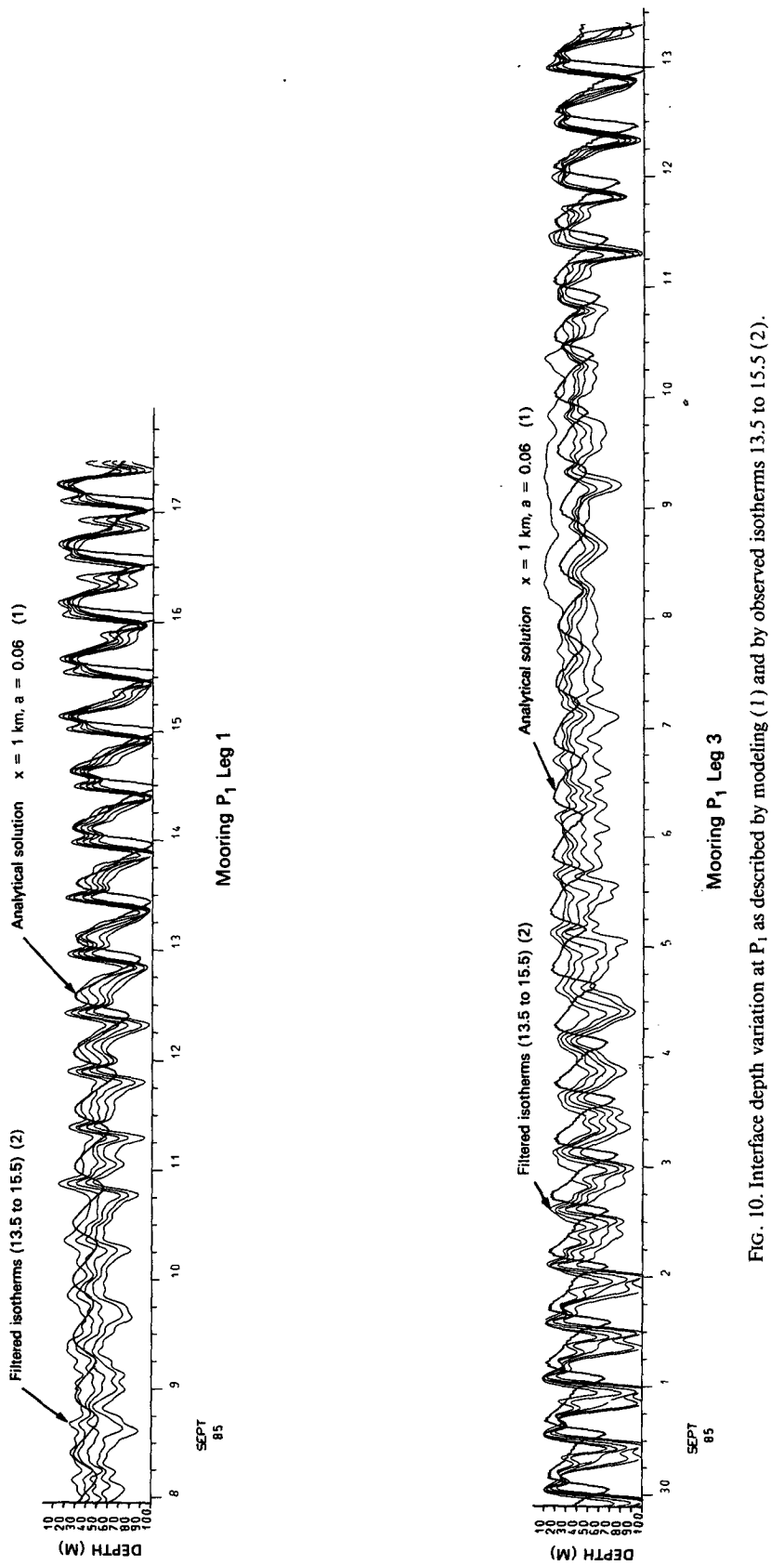


FIG. 10. Interface depth variation at $P_1$ as described by modeling (1) and by observed isotherms 13.5 to 15.5 (2).

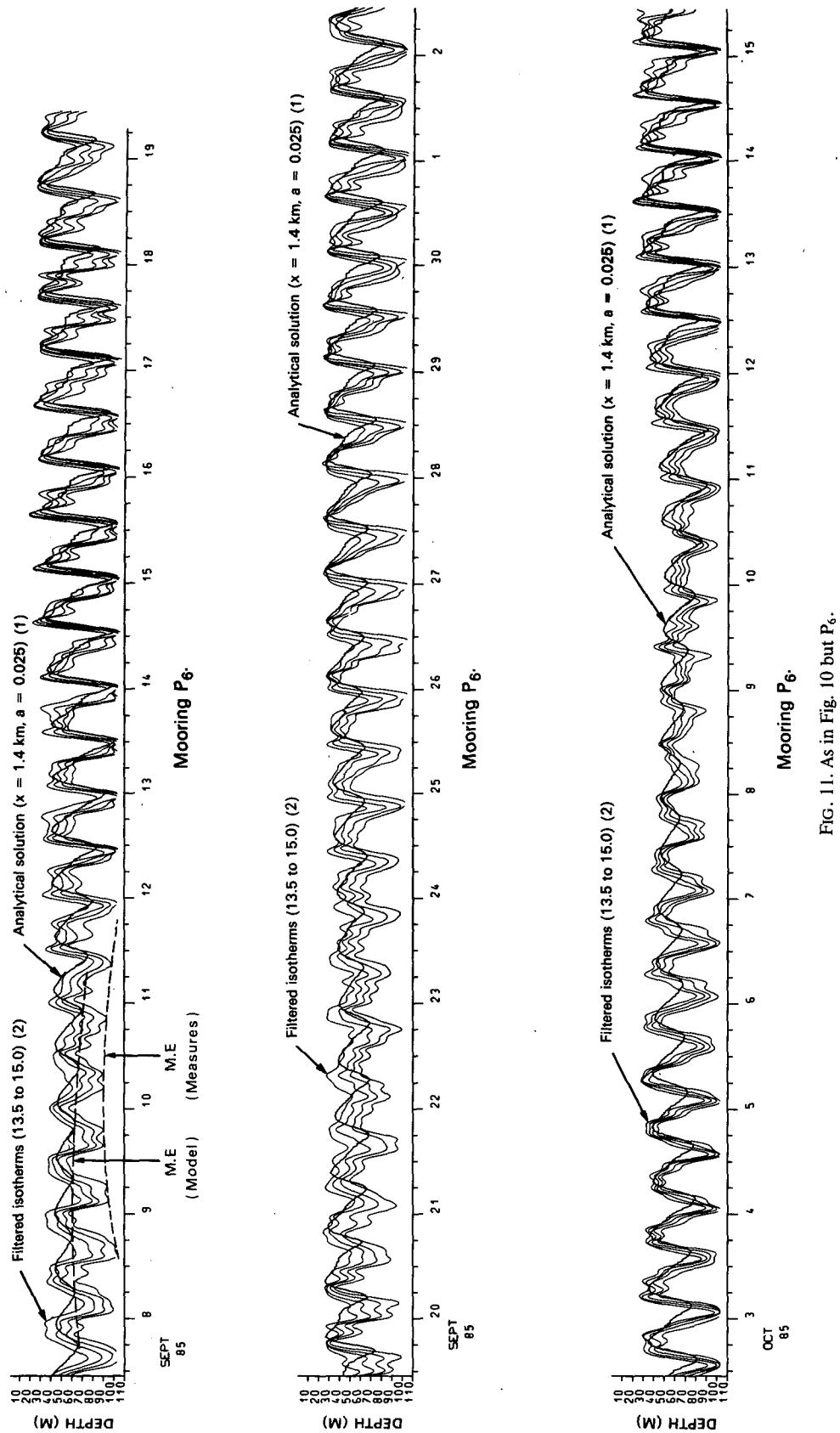


FIG. 11. As in Fig. 10 but $P_6$.

of a basin (Fig. 3), it is possible that the internal wave measured at $P_1$ corresponds, for example, to an interference between waves from $A_1$ and $A_2$ (Fig. 3).

2) RESULTS OF THE MODEL AT $P_6$ (FIG. 11)

The results for $P_6$ from 7 September to 16 October are similar in form and inferior in tidal range to those for $P_1$ (this is due to the difference in degree of slope near the two points: $a = 0.025$ at $P_6$ and $a = 0.06$ at $P_1$).

The superimposition of the model and the data indicates a greater phase difference than at $P_1$: according to the data, the September neap tide is centered around 0600 h on 10 September, whereas the model gives a neap tide centered around 1200 h on 9 September (Fig. 11).

It would seem that the wave measured at $P_6$ came from a generation point much further away. This could explain the difference in tidal range observed between the model and the data, if it is assumed that the generation point is further south in an area where the degree of slope is of the same order as at $P_1$.

## 4. Conclusion

The analytical model describes a two-layer vertical thermal structure at points on the shelf at a distance $x$ from the continental shelf break of the Bay of Biscay. It is based on highly simplified equations in which only the internal wave advection by the barotropic current is taken into account.

The solution obtained represents the change over time of the interface at a point on the continental shelf; this solution has been tested against temperature data from two points on the Bay of Biscay shelf about 1 km from the continental edge of the slope. These measurements taken during the ONDINE 85 cruise, cover one and a half months of observations, September to mid-October 1985.

The good fit of the model to field data confirms that the advection term of the internal wave by the barotropic wave is the major factor of the wave deformation during its propagation on the shelf.

The main positive aspects of the comparison can be summarized as follows: the model correctly gives the order of size of the internal wave tidal range at spring tides (approximately 80 m) and neap tides (approximately 20 m). The shape of the interface obtained from the model, at one kilometer from the shelf break corresponds to the shape of the isotherms, which are representative of the thermocline at the two measuring points. Moreover, the variation over time of the shape of this interface over several spring–neap cycles generally fits the observations.

The main differences between model and data result from poor understanding of the areas of internal movement generation, and of the vertical two-layer thermal structure model. In addition, the model is unidirectional, whereas the observations probably indicate the interaction of several waves over the area as a whole.

The model can be improved by using the results of a bidimensional numerical model, which gives more precise knowledge of the generation areas. Similarly, an extension of the vertical three-layer thermal structure should give a better fit between model and data for neap tide periods. However, this model can be used only in the vicinity of the shelf break, because the model contains no damping terms, the model is unidirectional and, last, because the approximation of a same phase celerity, $C_1$, for the wave $M_2, S_2, N_2, K_2$ is available only for points near the generation area.

In any case, the main interest of this model lies in the simplicity of its application from the numerical point of view, making it possible to obtain the temporal variation of the interface over a long period. (The simulation lasted one and a half months in the present case.)

## REFERENCES


Apel, 1985a: Nonlinear wave evolution in the Sulu Sea. *J. Phys. Oceanogr.*, **15**, 1613–1624.

——, 1985b: The Sulu Sea internal soliton experiment. *J. Phys. Oceanogr.*, **15**, 1625–1651.

Baines, P. G., 1982: On internal tide generation model. *Deep–Sea Res.*, **29**, 307–338.

Heathershaw, A. D., A. L. New and P. D. Edwards, 1987: Internal tides and sediment transport at the shelf break in the Celtic Sea. *Contin. Shelf Res.*, **7**(5), 485–517.

Mazé, R., 1983: Mouvements internes induits dans un golfe par le passage d'une dépression et par la marée. Application au Golfe de Gascogne. Thèse de Doctorat ès Sciences Physiques. Université de Bretagne Occidentale, Brest, 320 pp.

——, 1987: Generation and propagation of non-linear internal waves induced by the tide over a continental slope. *Contin. Shelf Res.*, **7**(9), 1079–1104.

——, Y. Camus and J. Y. Le Tareau, 1986: Formation de gradients thermiques à la surface de l'océan, au-dessus d'un talus, par interaction entre les ondes internes et le mélange dû au vent. *J. Cons. Int. Explor. Mer*, **42**, 221–240.

New, A. L., 1988: Internal tidal mixing in the Bay of Biscay. *Deep–Sea Res.*, **35**(5), 691–709.

Osborne, A. R., and T. L. Burch, 1980: Internal solitons in the Andaman Sea. *Sciences*, **208**, 451–460.

Pingree, R. D., D. K. Griffiths and G. T. Mardell, 1983: The structure of the internal tide at the Celtic Sea Shelf-Break. *J. Mar. Biol. Assoc. U.K.*, **64**, 99–113.

——, and G. T. Mardell, 1985: Solitary internal waves in the Celtic Sea. *Progress in Oceanography*, Vol. 14, Pergamon, 431–441.

——, —— and A. L. New, 1986: Propagation of internal tides from the upper slope of the Bay of Biscay. *Nature*, **321**, 154–158.

Willmott, A. O., 1987: A numerical model for the generation of tidally forced non-linear internal waves over topography. *Contin. Shelf Res.*, **7**(5), 457–484.